J Solid State Electrochem (2007) 11: 323–334
DOI 10.1007/s10008-005-0084-9

REVIEW

Joo-Young Go · Su-Il Pyun

A review of anomalous diffusion phenomena at fractal interface for diffusion-controlled and non-diffusion-controlled transfer processes

Received: 7 August 2005 / Revised: 27 October 2005 / Accepted: 17 November 2005 / Published online: 10 January 2006

Abstract This article reviewed anomalous diffusion phenomena coupled with facile and sluggish charge-transfer reactions at fractal interface. Firstly, the generalised diffusion equation (GDE) involving a fractional derivative which describes diffusion towards and from fractal interface was briefly introduced. And then, anomalous diffusion coupled with facile charge-transfer reaction at fractal interface, i.e., diffusion-controlled transfer process across fractal interface, was mathematically examined by the generalised Cottrell, Sand, Randles-Sevcik and Warburg equations theoretically derived from the analytical solutions to the GDE under the semi-infinite boundary condition. Finally, in order to provide a guideline in analysing anomalous diffusion coupled with sluggish charge-transfer reaction at fractal interface, i.e., non-diffusion-controlled transfer process across fractal interface, this review covered the recent researches into the effect of surface roughness on non-diffusion-controlled transfer process within the intercalation electrodes.

Keywords Anomalous diffusion · Fractal interface · Generalised diffusion equation · Diffusion-controlled transfer process · Non-diffusion-controlled transfer process

Abbreviations BC: Boundary condition · CPE: Constant phase element · CTRW: Continuous time random walk · EIS: Electrochemical impedance spectroscopy · FDE: Fractional diffusion equation · GDE: Generalised diffusion equation · IC: Initial condition · LSV: Linear sweep voltammogram · MC: Monte Carlo · MCS: Monte Carlo step · MH_x: Metal hydride · MSD: Mean squared displacement · Ox: Oxidised species · PCT: Potentiostatic current transient · Red: Reduced species · TEISI: Transfert d'Energie sur Interface à Similitude Interne

J.-Y. Go · S.-I. Pyun (✉)
Department of Materials Science and Engineering,
Korea Advanced Institute of Science and Technology,
373-1, Guseong-dong, Yuseong-gu,
Daejeon, 305-701, Republic of Korea
e-mail: sipyun@webmail.kaist.ac.kr
Tel.: +82-42-8693319
Fax: +82-42-8693310

Introduction

Ordinary diffusion which obeys Fick's second law is characterised by the linear time dependence of a mean squared displacement (MSD) expressed as:

$$\langle r^2(t)\rangle \propto t \tag{1}$$

where r is the displacement of the diffusion species after the time t. However, if the MSD does not obey Eq. (1) but has a power law dependence on t given as:

$$\langle r^2(t)\rangle \propto t^{2/d_W} \tag{2}$$

where d_W is the anomalous diffusion exponent (d_W>1), the processes are termed anomalous diffusion, which no longer follows Fick's second law.

Actually, anomalous diffusion is observed in a wide range of different fields: Richardson turbulent diffusion [1–4], charge carrier transport in amorphous semiconductors [5–11], diffusion of a scalar tracer in an array of convection rolls [12], dynamics of a bead in a polymeric network [13, 14], transport in turbulent plasma [15], collective slip diffusion on solid surfaces [16], bulk-surface exchange controlled dynamics in porous glasses [17–19], diffusion in fractal media [20–28], diffusion towards and from fractal interface (diffusion in a dense object with fractal surface) [29–38] etc. In order to describe anomalous diffusion theoretically, many researchers have extensively used the continuous time random walk (CTRW) model [39, 40] as well as kinetic equations with a fractional derivative [40–42]. Fractional kinetic equations allow one to explore various boundary conditions and to study the phenomena of various kinetic processes in external fields, so fractional kinetic equations have recently attracted more attention than CTRW model as a powerful tool for the description of anomalous diffusion.

Diffusion towards and from fractal interface, especially, has been of interest in electrochemistry because it provides crucial clues to solve problems arising from the irregular electrode/electrolyte interface in various electrochemical

processes. Thus, there have been considerable theoretical and experimental researches into diffusion towards and from the fractal electrode/electrolyte interface by using electrochemical methods such as potentiostatic current transient (PCT) [33, 38, 43–46], linear sweep/cyclic voltammetric [34, 38, 47–49] and alternating current (AC) impedance [50–52] experiments. In most cases, various electrochemical responses which result from diffusion towards and from the fractal electrode/electrolyte interface have been analysed based upon the condition of the diffusion-control which assumes that the rate-controlling step is the diffusion process.

When the electrochemical process is purely controlled by the diffusion process, the electrochemical responses at the fractal electrode/electrolyte interface obey the generalised Cottrell, Sand, Randles-Sevcik and Warburg relations [38]. These generalised equations can theoretically be derived from the analytical solutions to the generalised diffusion equation (GDE) involving the fractional derivative [32, 38, 53–55], which is sometimes termed the fractional diffusion equation (FDE) in the literature, under the diffusion-controlled and semi-infinite boundary conditions. In the literature, they were theoretically verified via Monte Carlo (MC) simulations of random walk [31, 33, 34, 36, 37, 56–61] and also experimentally justified by the diffusion-controlled electrochemical methods [33, 34, 38, 43–52].

Unfortunately, in the case of the non-diffusion-controlled electrochemical process, the generalised equations derived under the diffusion-controlled and semi-infinite diffusion boundary conditions are not valid any more. Nevertheless, relatively little attention has been paid to the electrochemical responses at the fractal electrode/electrolyte interface under the non-diffusion-controlled boundary condition, e.g., the constraint of mixed control, because of its complicated schemes.

There have been some attempts to investigate the electrochemical responses at the fractal electrode/electrolyte interface where the constraint of mixed control is imposed. de Levie and Vogt [62] derived explicit equations for the current response to a potential step, i.e., the PCT, at a fractal interface with self-similar scaling property, by employing the Laplace transform method, in case a sluggish charge-transfer process is operative. Furthermore, Kant and Rangarajan [63] formulated kinetic theories of the diffusion process involving finite charge-transfer rates using the perturbation approach, and especially the authors provided analytical expressions for the PCT at fractal interfaces with various morphological features. However, the above work is oversimplified [62] or quite theoretically oriented [63], so it is very difficult to completely or straightforwardly grasp the behaviours of the PCT at the fractal interfaces when diffusion is coupled with sluggish charge-transfer reaction.

Recently, Pyun and his co-workers [61, 64–66] have systematically studied how the surface roughness affects atomic diffusion within the intercalation electrodes under the non-diffusion-controlled constraint by using theoretical [61, 64] and experimental [65, 66] methods: hydrogen transport through the hydride-forming electrode under the constraint of atomic diffusion coupled with interfacial charge-transfer [61, 66] and lithium transport through the $Li_{1-\delta}CoO_2$ electrode under the cell-impedance-controlled constraint [64, 65].

The works of Pyun et al. may have attracted attention to the researchers who devote themselves to investigating kinetics of transfer processes in various systems because these works first manifested the fractal-to-flat transition and vice versa under the constraint of mixed control [61] and they gave a guideline in analysing the electrochemical responses at fractal interface in a realistic regime.

The present article deals with anomalous diffusion towards and from fractal interface. This review article is composed of the following: the article starts off with a brief introduction of the GDE, which mathematically describes diffusion towards and from fractal interface, and then overviews the electrochemical responses at fractal interface where the diffusion-controlled constraint is imposed by using the analytical solutions to the GDE. Finally, the electrochemical responses at fractal interface where the non-diffusion-controlled constraint is imposed are discussed in detail for the hydrogen transport under the constraint of hydrogen diffusion coupled with interfacial charge-transfer [67–71] and for the lithium transport under the cell-impedance-controlled constraint [46, 72–75].

Mathematical description of diffusion towards and from fractal interface: GDE or FDE

The modelling of diffusion in fractal media and diffusion towards and from fractal interface is one of the most significant applications of fractional derivatives [76]. Although each fractional differential equation to describe diffusion in fractal media and diffusion towards and from fractal interface is equally termed the GDE (or FDE), in this review, we considered the GDE mean the fractional differential equation to describe diffusion towards and from fractal interface.

For the description of transfer processes across fractal interface (in the sense of Mandelbrot [77]), Le Mehaute [29, 30] proposed the Transfert d'Energie sur Interface à Similitude Interne (TEISI) model which treats the thermodynamics of irreversible processes. In the linear approximation of the thermodynamics of irreversible processes, the macroscopic flow of an extensive quantity across fractal interface $J(t)$ is described by a generalised transfer equation which is expressed as:

$$\frac{d^{(1/d_F)-1}}{dt^{(1/d_F)-1}} J(t) = K_0 \Delta X(t) \tag{3}$$

where d_F is the fractal dimension, K_0 is the constant and $\Delta X(t)$ represents the local driving force.

The GDE involving the fractional derivative was explicitly introduced in physics by Nigmatullin [32] to describe diffusion across the surface with fractal geometry and was mathematically studied by Wyss [53], Schneider and Wyss

[54] and Mainardi [55]. In the simplest case of spatially one-dimensional diffusion of lithium, it is expressed as [38]:

$$\frac{\partial^{3-d_F} c(x,t)}{\partial t^{3-d_F}} = \widetilde{D}^* \frac{\partial^2 c(x,t)}{\partial x^2} \quad (2 \le d_F < 3) \tag{4}$$

where $c(x,t)$ is the local concentration of diffusing species, x the distance from fractal interface, $\widetilde{D}^*$ the fractional diffusivity defined as $K^{4-2d_F} A_{ea}^{d_F-2} \widetilde{D}^{3-d_F}$ (K is a constant related to d_F of fractal interface, A_{ea} is the time-independent electrochemically active area of flat interface and $\widetilde{D}$ represents the chemical diffusivity of diffusing species) and $\partial^v/\partial t^v$ means the Riemann–Liouville mathematical operator of the fractional derivative:

$$\frac{\partial^v y}{\partial t^v} = \frac{1}{\Gamma(1-v)} \frac{d}{dt} \int_0^t \frac{y(\xi)}{(t-\xi)^v} d\xi \tag{5}$$

where $\Gamma(1-\nu)$is the gamma function of $(1-\nu)$.

The procedure of the mathematical derivation of Eq. (4) was rigorously checked by Dassas and Duby [38]. Based upon the concept of the generalised transfer equation (Eq. 3), the flow at fractal interface $J_F(x,t)$ is given as [38]:

$$J_F(x,t) = \frac{\partial}{\partial t} \left[\left\{ \widetilde{D}_F(t)^* \frac{\partial c(x,t)}{\partial x} \right\} \right] \tag{6}$$

where * is the convolution operator and $\widetilde{D}_F(t)$ represents the time-dependent diffusivity defined as:

$$\widetilde{D}_F(t) = \widetilde{D}^* \frac{t^{2-d_F}}{\Gamma(3-d_F)} \tag{7}$$

By using Eq. (6), diffusion towards and from fractal electrode is mapped to a one-dimensional diffusion in Euclidean space as follows:

$$A_{ea} J_F(x,t) = A_F(t) J_E(x,t) \tag{8}$$

where $A_F(t)$ is the time-dependent area of fractal interface defined as $k^{2-d_F} A_{ea}^{d_F/2} (\widetilde{D}t)^{(2-d_F)/2}$ (k is a dimensionless constant) and $J_E(x,t)$ represents the flow at planar interface given by Fick's first law. Consequently, this mapping process leads to the generalisation of Fick's second law (Eq. 4) by the substitution of $\partial^{3-d_F}/\partial t^{3-d_F}$ and $\widetilde{D}^*$ for $\partial/\partial t$ and $\widetilde{D}$, respectively. When d_F equals 2, Eq. (4) becomes the usual Fick's second law for diffusion towards and from flat electrode/electrolyte interface.

Diffusion towards and from fractal interface coupled with facile charge-transfer reaction (diffusion-controlled condition)

Analytical solutions to the GDE

Now let us examine the analytical solutions to the GDE of Eq. (4) at the potentiostatic, galvanostatic, linear sweep/cyclic voltammetric and AC impedance experiments under the assumption of the semi-infinite diffusion coupled with facile charge-transfer reaction. These four analytical solutions for the potentiostatic, galvanostatic, linear sweep/cyclic voltammetric and AC impedance experiments refer to the generalised Cottrell, Sand, Randles-Sevcik and Warburg equations, respectively. Recently, their derivation was rigorously checked by Dassas and Duby [38] using Laplace transform of the fractional derivative.

For the derivation, the initial condition (IC) and the boundary condition (BC) for the semi-infinite diffusion are given as:

$$\text{IC:} \quad c(x,0) = c^b \quad \text{for } 0 \le x < \infty \tag{9}$$

$$\text{BC:} \quad c(\infty,t) = c^b \quad \text{at } t \ge 0 \text{ (semi} - \text{infinite constraints)} \tag{10}$$

where c^b is the bulk concentration of the diffusing species.

Generalised Cottrell equation

During the potentiostatic experiment, the BC at the electrode/electrolyte interface for the diffusion-controlled condition is given as:

$$\text{BC: } c(0,t) = 0 \quad \text{at } t > 0 \quad \text{(potentiostatic constraints)} \tag{11}$$

From the Laplace transforms of Eqs. (4), (9), (10) and (11), the generalised Cottrell equation which describes the response of the current I on the potential step ΔE applied on the electrode is obtained as the following equation [38]:

$$\begin{aligned} I(t) &= \frac{zFA_{ea}\sqrt{\widetilde{D}^*}c^b}{\Gamma\left(\frac{3-d_F}{2}\right)} t^{-(d_F-1)/2} \\ &= \frac{zFA_{ea}^{d_F/2} K^{2-d_F} \tilde{D}^{(3-d_F)/2} c^b}{\Gamma\left(\frac{3-d_F}{2}\right)} t^{-(d_F-1)/2} \end{aligned} \tag{12}$$

where $I(t)$ is the current as a function of t, z is the valence of the diffusing species and F represents the Faraday constant (=96,487 C mol^{-1}). The Cottrell equation for ordinary diffusion is retrieved for d_F=2.

Figure 1 gives the PCTs theoretically determined from Eq. (12) as a function of d_F. Considering lithium diffusion in $Li_{1-\delta}CoO_2$ film electrode, the values of the parameters involved in Eq. (12) were taken as z=1, $A_{ea} = 1\,cm^2$, K=1, $\widetilde{D} = 1 \times 10^{-10}\,cm^2\,s^{-1}$ and $c^b = 1 \times 10^{-3}\,mol\,cm^{-3}$ [46]. The PCTs clearly exhibited a linear relationship between the logarithm of current and the logarithm of time showing the power exponent of $-(d_F-1)/2$.

Generalised Sand equation

During the galvanostatic experiment, the BC at the electrode/electrolyte interface for the diffusion-controlled condition is given as:

$$\text{BC: } \left(\frac{\partial c(x,t)}{\partial x}\right)_{x=0} = -\frac{I_{app}}{zFA_{ea}\widetilde{D}_F(t)} \text{ at } t>0 \quad \text{(galvanostatic constraint)} \tag{13}$$

where I_{app} is the applied current.

From the Laplace transforms of Eqs. (4), (9), (10) and (13), the generalised Sand equation, which describes the relationship between the constant I_{app} applied on the electrode and the transition time τ which is the time needed for the concentration of diffusing species to drop to zero at the electrode/electrolyte interface, is obtained as the following equation [38]:

$$I_{app} = zFA_{ea}\sqrt{\widetilde{D}^*}c^b\Gamma\left(\frac{d_F+1}{2}\right)\tau^{-(d_F-1)/2} = zFA_{ea}^{d_F/2}K^{2-d_F}\widetilde{D}^{(3-d_F)/2}c^b\Gamma\left(\frac{d_F+1}{2}\right)\tau^{-(d_F-1)/2} \tag{14}$$

The Sand equation for ordinary diffusion is retrieved for d_F=2.

Figure 2 shows the plot of I_{app} vs τ theoretically determined from Eq. (16) as a function of d_F by taking the values of the parameters involved in Eq. (16) as z=1, A_{ea}=1 cm^2, K=1, $\widetilde{D} = 1 \times 10^{-10}\,cm^2\,s^{-1}$ and $c^b = 1 \times 10^{-3}\,mol\,cm^{-3}$. It is clearly observed that a linear relationship between the logarithm of current and the logarithm of transition time exhibited the power exponent of -(d_F−1)/2.

Generalised Randles-Sevcik equation

In order to obtain the generalised Randles-Sevcik equation, let us consider the redox reaction between the oxidised species Ox and the reduced species Red, i.e., Ox+ze=Red, with a solution initially containing only Ox whose concentration is equal to be c^b. The electrode is initially subjected to an initial electrode potential E_{ini} where no reaction takes place.

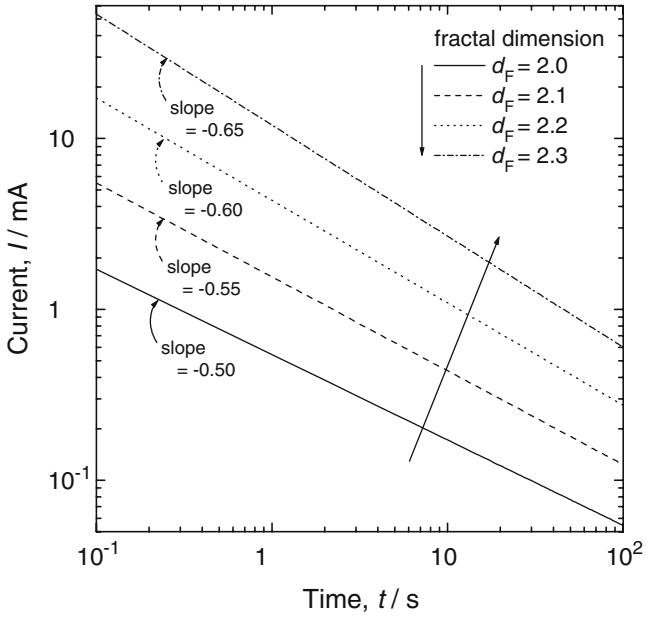

Fig. 1 Plot of the current I vs the time t theoretically determined from Eq. (12) as a function of the fractal dimension d_F for diffusion in the fractal electrode during the potentiostatic experiment. The values of the parameters involved in Eq. (12) were taken as z=1, A_{ea}=1 cm^2, K=1, $\widetilde{D} = 1 \times 10^{-10}\,cm^2\,s^{-1}$ and $c^b = 1 \times 10^{-3}\,mol\,cm^{-3}$

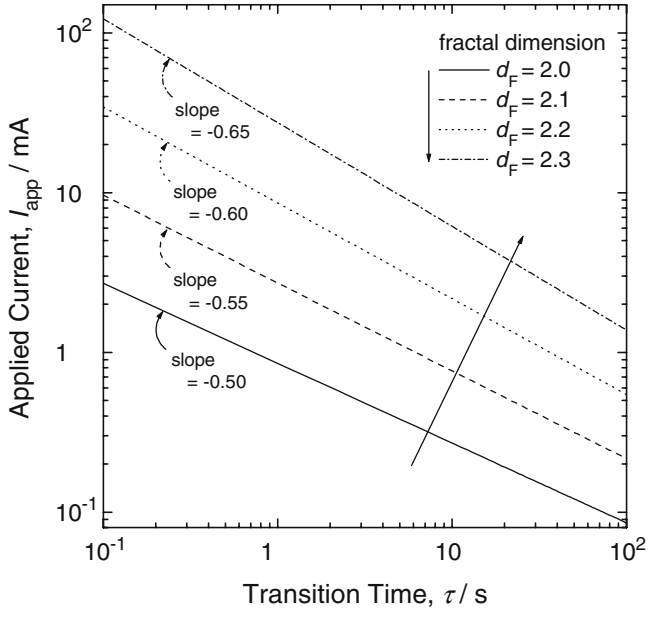

Fig. 2 Plot of the applied current I_{app} vs the transition time τ theoretically determined from Eq. (14) as a function of the fractal dimension d_F for diffusion in the fractal electrode during the galvanostatic experiment. The values of the parameters involved in Eq. (14) were taken as z=1, A_{ea}=1 cm^2, K=1, $\widetilde{D} = 1 \times 10^{-10}$ cm^2 s^{-1} and $c^b = 1 \times 10^{-3}\,mol\,cm^{-3}$

For the sake of simplicity, it is assumed that the diffusivities of Ox and Red are equal, i.e., $\widetilde{D} = \widetilde{D}_{Ox} = \widetilde{D}_{Red}$. During the linear sweep/cyclic voltammetric experiments, the potential is linearly increased or decreased with $E(t) = E_{ini} \pm \nu t$, where $E(t)$ is the electrode potential as a function of t, ν is the potential scan rate and the signs "+" and "–" represent anodic scan and cathodic scan, respectively. Under the assumption that the redox couple is reversible, the surface concentrations of Ox and Red, i.e., $c_{Ox}(0,t)$ and $c_{Red}(0,t)$, respectively, are always determined by the electrode potential E expressed as the following equation which is derived from the Nernst equation:

$$E = E_{1/2} + \frac{RT}{zF} \ln\left(\frac{c_{Ox}(0,t)}{c_{Red}(0,t)}\right) \tag{15}$$

where $E_{1/2}$ means the half-wave potential, i.e., the potential bisecting the distance between anodic and cathodic peaks in a cyclic voltammogram, R is the gas constant (=8.314 J mol^{-1} K^{-1}) and T is the temperature.

Under this circumstance, the generalised Randles–Sevcik equation which explains the power dependence of the peak current I_{peak} on ν can be derived from Eq. (4) as follows [38]:

$$\begin{aligned} I_{peak} &= \frac{0.2518(zF)^{3/2} A_{ea}\sqrt{\widetilde{D}^*}c^b}{(RT)^{1/2}}\Gamma\left(\frac{d_F-1}{2}\right)\nu^{(d_F-1)/2} \\ &= \frac{0.2518(zF)^{3/2} A_{ea}^{d_F/2} K^{2-d_F}\widetilde{D}^{(3-d_F)/2}c^b}{(RT)^{1/2}}\Gamma \\ &\quad \left(\frac{d_F-1}{2}\right)\nu^{(d_F-1)/2} \end{aligned} \tag{16}$$

The Randles-Sevcik equation for ordinary diffusion is retrieved for d_F=2.

Figure 3 presents the plot of I_{peak} vs ν theoretically determined in Eq. (16) as a function of d_F by taking the values of the parameters involved in Eq. (16) as z=1, A_{ea}=1 cm^2, K=1, $\widetilde{D} = 1 \times 10^{-10}$ cm^{2}s^{-1}, $c^b = 1 \times 10^{-3}$ mol cm^{-3} and T=298 K. The power dependence of I_{peak} on ν with the power exponent of (d_F–1)/2 can be confirmed in Fig. 3.

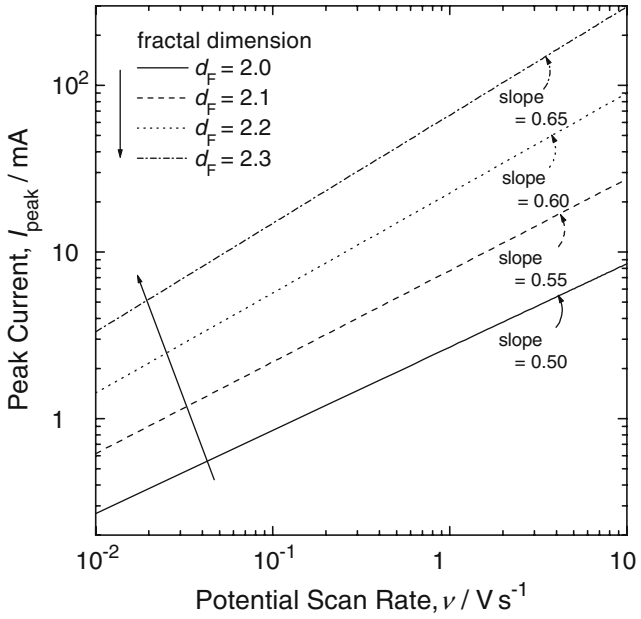

Fig. 3 Plot of the peak current I_{peak} vs the potential scan rate ν theoretically determined from Eq. (16) as a function of the fractal dimension d_F for diffusion in the fractal electrode during the linear sweep/cyclic voltammetric experiments. The values of the parameters involved in Eq. (16) were taken as z=1, A_{ea}=1 cm^2, K=1, $\widetilde{D} = 1 \times 10^{-10}$ cm^2 s^{-1}, $c^b = 1 \times 10^{-3}$ mol cm^{-3} and T=298 K

Generalised Warburg equation

The electrochemical impedance of diffusion in a spatially restricted layer has extensively been studied as a tool for the electrochemical characterisation of the intercalation electrodes whose one side is impermeable [78–83]. In AC impedance experiment, i.e., electrochemical impedance spectroscopy (EIS), a small sinusoidal signal of $E(t)$ superimposed onto the electrode with the reversible potential E_{rev} is given as:

$$E(t) = E_{rev} + \varepsilon \sin \omega t \tag{17}$$

where ε is a constant which represents a perturbation amplitude (usually 5 mV in AC impedance experiment) and ω means the angular frequency.

Under this circumstance, the diffusion impedance $Z_d(\omega)$ under the impermeable boundary condition can be derived from Eq. (4) as follows [82, 83]:

$$Z_d(\omega) = \frac{L}{zFA_{ea}\widetilde{D}^*}\left(\frac{dE}{dc}\right)\frac{\coth\left[(j\omega)^{(3-d_F)}L^2\Big/\widetilde{D}^*\right]^{1/2}}{\left[(j\omega)^{(d_F-1)}L^2\Big/\widetilde{D}^*\right]^{1/2}} \tag{18}$$

where L is the thickness of the electrode. $Z_d(\omega)$ for a planar electrode with the flat surface is retrieved for d_F=2.

Figure 4a,b gives the typical AC impedance spectra in Nyquist representation and the variations of the phase angle θ with logω, respectively, theoretically calculated from Eq. (18) as a function of d_F by assuming $L = 1 \times 10^{-5}$ cm, z=1, A=1 cm^2, $\widetilde{D} = 1 \times 10^{-10}$ cm^{2}s^{-1} and (dE/dc)=20 V cm^3 mol^{-1}. The AC impedance spectrum obtained from the fractal electrode deviates more considerably from the ideal behaviour for d_F=2 with rising d_F.

In Fig. 4b, it should be noted that $Z_d(\omega)$ clearly shows a power law behaviour of frequency dispersion, with the constant value of θ in the high-frequency range. This means the appearance of the Warburg impedance in the high-frequency regime, $\omega >> \widetilde{D}\Big/L^2$. As a matter of fact,

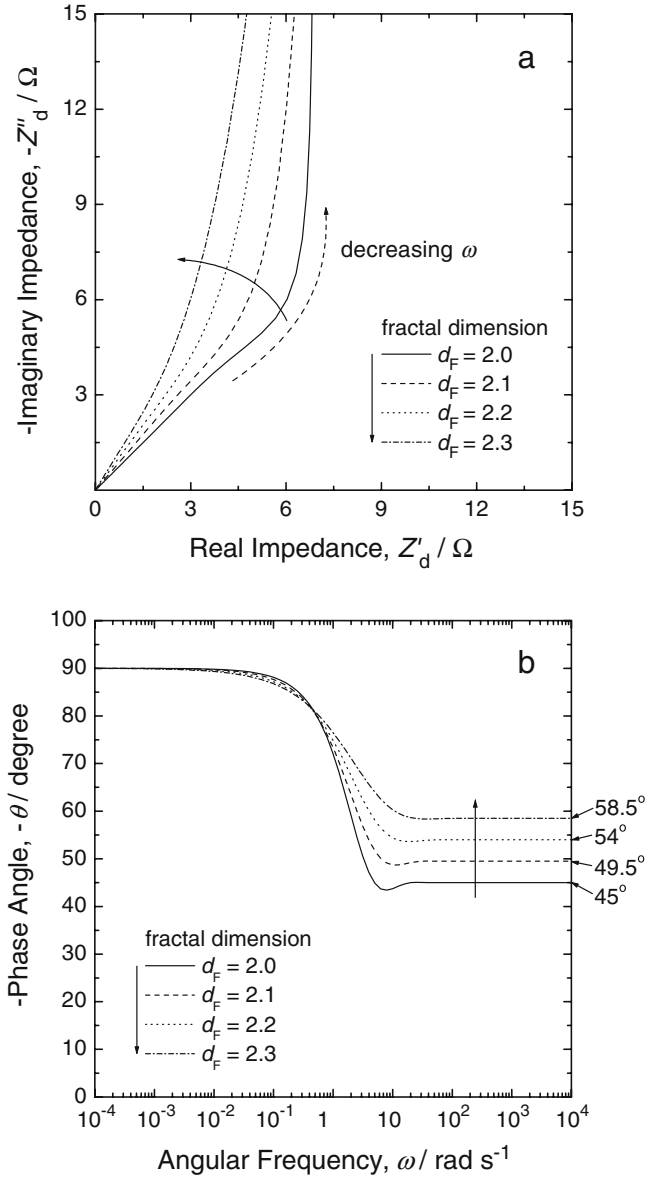

Fig. 4 **a** Nyquist plots of the AC impedance spectrum and **b** bode plots of the phase angle θ vs the logarithm of angular frequency logω theoretically determined from Eq. (18) as a function of the fractal dimension d_F for diffusion in the fractal electrode during the AC potential oscillation experiment. The values of the parameters involved in Eq. (18) were taken as $L = 1 \times 10^{-5}$ cm, z=1, A=1 cm^2, $\widetilde{D} = 1 \times 10^{-10}$ cm^2 s^{-1} and (dE/dc)=20 V cm^3 mol^{-1} [83]

at high frequencies, Eq. (18) reduces to the generalised Warburg equation given as [38]:

$$Z_d(\omega) = \frac{1}{zFA_{ea}\sqrt{\widetilde{D}^*}}\left(\frac{dE}{dc}\right)(j\omega)^{-(d_F-1)/2} \tag{19}$$

which represents the constant phase element (CPE) behaviour whose exponent is (d_F−1)/2.

Diffusion towards and from fractal interface coupled with sluggish charge-transfer reaction (non-diffusion-controlled condition)

Hydrogen transport under the constraint of hydrogen diffusion coupled with interfacial charge-transfer

Recently, it has been reported [67–71] that hydrogen transport through the hydride-forming electrodes such as Pd and metal hydrides (MH_x) proceeds under the condition where hydrogen diffusion in the electrode is coupled with the charge-transfer reaction at the electrode/electrolyte interface, when the hydrogen extraction potential is kept below a certain value during the potential jump and the potential scan rate ν is kept below a critical value during the potential scan. Under this constraint of mixed control where the rate of the interfacial charge-transfer is determined by the Butler–Volmer equation, Lee and Pyun [61] investigated a transport phenomenon in the hydride-forming electrode with fractal surface by using the kinetic MC simulation of random walk.

Now we will introduce Lee and Pyun's theoretical work [61] since they first manifested the fractal-to-flat transition and vice versa under the constraint of mixed control and gave a guideline in analysing the experimental data of the PCT and linear sweep voltammogram (LSV) measured on the hydride-forming electrodes with fractal surfaces.

Firstly, in order to obtain the self-affine fractal interface boundary between the electrode and the electrolyte, Lee and Pyun [61] employed the Weierstrass function f_{WS} expressed as [60, 84]:

$$f_{WS}(y) = \sum_{j=1}^{N} b^{(d_{F,sa}-2)j}\cos\left(b^j y\right) \tag{20}$$

where $d_{F,sa}$ denotes the self-affine fractal dimension of the function and b and N are the constants. Lee and Pyun [61] constructed the self-affine fractal profiles with $d_{F,sa}$=1.3 and 1.5 by taking the values of b and N as 1.5 and 50, respectively. Considering that the diffusing atoms/ions sense the self-similar scaling property of the self-affine fractal surface due to their random motion in all directions [46, 49, 60], Lee and Pyun [61] estimated the self-similar fractal dimensions $d_{F,ss}$ of the constructed self-affine fractal profiles with $d_{F,sa}$=1.3 and 1.5 to be $d_{F,ss}$=1.32 and 1.47, respectively, using a triangulation method [60, 85].

Afterwards, Lee and Pyun [61] theoretically computed the PCT and the LSV from the flat and fractal MH_x electrodes by using the kinetic MC simulation of random walk under the constraint of hydrogen diffusion coupled with the interfacial charge-transfer along with the semi-infinite constraint. In their calculation, the electrode potential curve for the hydride-forming electrode, i.e., the plot of E vs the dimensionless hydrogen content x in MH_x, was derived from the Nernst equation. In addition, the dimensionless jump probability of hydrogen W_{tr} across the electrode/elec-

trolyte interface was defined by the same form as the Butler-Volmer equation:

$$W_{\mathrm{tr}} = f\left[\exp\left(\frac{(1-\alpha)F}{RT}\left(E_{\mathrm{app}} - E(t)\right)\right) - \exp\left(-\frac{\alpha F}{RT}\left(E_{\mathrm{app}} - E(t)\right)\right)\right] \quad (0 \le W_{\mathrm{tr}} < 1) \tag{21}$$

where f designates the dimensionless conversion factor which simply represents the exchange current I_0 or the rate constant of charge-transfer k^0 in I_0, α the transfer coefficient for hydrogen reduction, 1–α the transfer coefficient for hydrogen oxidation and E_{app} the applied potential. Here, f was arbitrarily taken as the value below unity, keeping in mind that the current under the constraint of mixed control is always lower in value than the current under the diffusion-controlled constraint [61]. Accordingly, W_{tr} in Eq. (21) is the dimensionless parameter with the value below unity $(0 \le W_{\mathrm{tr}} < 1)$.

Figures 5 and 6 give on a logarithmic scale the resulting PCTs and plots of I_{peak} vs ν, respectively, calculated from the flat MH_x electrode with $d_{\mathrm{F,ss}}$=1.0 and the fractal MH_x electrodes with $d_{\mathrm{F,ss}}$=1.32 and 1.47 under the constraint of hydrogen diffusion coupled with interfacial charge-transfer with $f = 2 \times 10^{-3}$. In Fig. 5, the logarithmic PCT computed from the flat MH_x electrode with $d_{\mathrm{F,ss}}$=1.0 showed a typical feature of the PCT under the constraint of mixed control [58, 71]: an absolute slope of log$I$ with log$t$ flatter than 0.5, followed by its monotonic increase with time. On the other hand, it is noticeable that an inflexion point appeared at $t \approx$1,200 MCS (Monte Carlo step) in both the PCTs simulated from the fractal MH_x electrodes with $d_{\mathrm{F,ss}}$=1.32 and 1.47.

In parallel, in Fig. 6 obtained from the LSVs calculated at various ν, I_{peak} determined from the flat MH_x electrode with $d_{\mathrm{F,ss}}$=1.0 was linearly proportional to ν to the power of 0.517 over the whole scan rate range. On the other hand, the plots of logI_{peak} vs logν obtained from the fractal MH_x electrodes with $d_{\mathrm{F,ss}}$=1.32 and 1.47 consisted of two straight lines who intersect at the transition potential scan rate: the LSVs from the fractal MH_x electrodes exhibited a less positive power dependence of I_{peak} on ν at ν above the transition potential scan rate, compared with the generalised Randles–Sevcik relation expressed in Eq. (16), viz., $I_{\mathrm{peak}} \propto \nu^{0.635}$ for $d_{\mathrm{F,ss}}$=1.32 and $I_{\mathrm{peak}} \propto \nu^{0.687}$ for $d_{\mathrm{F,ss}}$=1.47. Subsequently, the values of logI_{peak} were linearly propor-

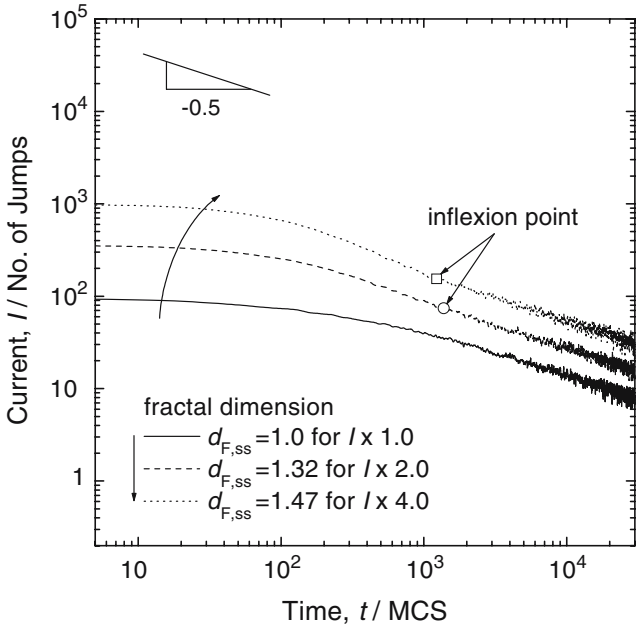

Fig. 5 Potentiostatic current transients on a logarithmic scale calculated from the flat MH_x electrode with $d_{\mathrm{F,ss}}$=1.0 and the fractal MH_x electrode with $d_{\mathrm{F,ss}}$=1.32 and 1.47 by jumping the initial electrode potential of 0.024 V to the hydrogen extraction potential of 0.08 V under the constraint of hydrogen diffusion coupled with interfacial charge-transfer with $f = 2 \times 10^{-3}$. For the sake of clear distinction between the simulated data, the values of I for $d_{\mathrm{F,ss}}$=1.32 and 1.47 were multiplied by the factors 2.0 and 4.0, respectively [61]

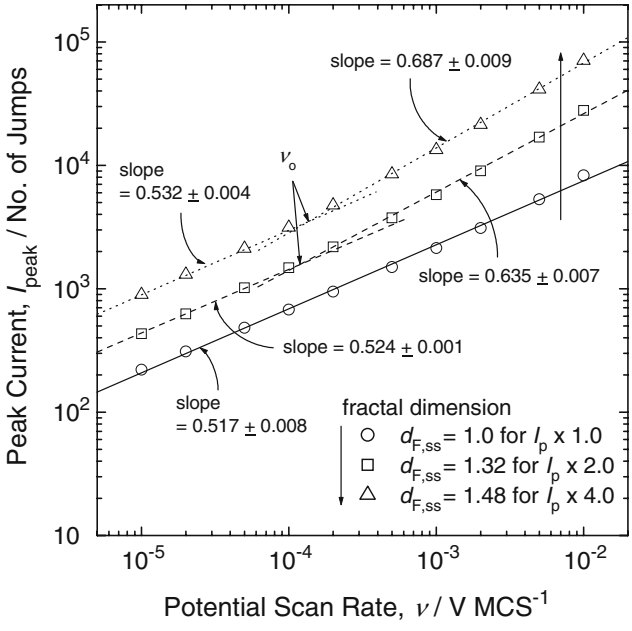

Fig. 6 Plots of the peak current I_{peak} vs the potential scan rate ν calculated from the flat MH_x electrode with $d_{\mathrm{F,ss}}$=1.0 and the fractal MH_x electrodes with $d_{\mathrm{F,ss}}$=1.32 and 1.47 by scanning the applied potential from −0.3 to 0.3 V at various ν from 1×10^{-5} to 1×10^{-2} V MCS^{-1} under the constraint of hydrogen diffusion coupled with interfacial charge-transfer with $f = 2 \times 10^{-3}$. For the sake of clear distinction between the simulated data, the values of I_{peak} for $d_{\mathrm{F,ss}}$=1.32 and 1.47 were multiplied by the factors 2.0 and 4.0, respectively [61]

tional to logν with slopes of 0.524 and 0.532 for $d_{F,ss}$=1.32 and 1.47, respectively, at ν below the transition potential scan rate. The values of the transition potential scan rate were determined to be approximately 1.3×10^{-4} V MCS^{-1} as well, as presented in Fig. 6.

Finally, Lee and Pyun [61] discussed the effect of the interfacial charge-transfer kinetics on the fractal-to-flat transition behaviour of atom transport based upon the simulated data. From the concentration profiles of hydrogen in the fractal MH_x electrode, it was suggested that under the constraint of mixed control, the inflexion point of the PCT in Fig. 5 and the transition potential scan rate of the plots of I_{peak} vs ν in Fig. 6 are caused by the fractal-to-flat transition and vice versa, respectively: namely, the inflexion point of the PCT corresponds to the temporal outer cut-off τ_0 of fractality, and the transition potential scan rate of the plots of I_{peak} vs ν corresponds just to the slow threshold scan rate ν_0 which characterises τ_0 during the potential scan.

Lee and Pyun [61] found that τ_0 and ν_0 determined under the constraint of mixed control were much longer and slower in value, respectively, than those values determined under the diffusion-controlled constraint. Furthermore, under the constraint of mixed control, the prolongation of τ_0 was observed as the values of the simulation parameters of f and ΔE increased in the PCT and the reduction of ν_0 appeared as the value of f increased in the LSV. These results were explained in terms of the growth rate of the diffusion layer by considering that the diffusion layer thickness serves as a yardstick length for probing the fractal topography of the electrode surface during hydrogen transport [33, 44]: the slow interfacial charge-transfer reaction decreases the growth rate of diffusion layer, thus making τ_0 and ν_0 longer and slower, respectively, under the constraint of mixed control.

From the rigorous theoretical study on the mixed-controlled hydrogen transport through the hydride-forming electrode by Lee and Pyun [61], we can recognise that the temporal cut-off ranges under the constraint of mixed control during the potentiostatic current transient and linear sweep voltammetric experiments are determined not only by the spatial cut-off range of fractality and the hydrogen diffusivity in the electrode, but also by the kinetic parameters, e.g., k^0, and the experimental variables, e.g., ΔE, governing the interfacial charge-transfer kinetics. Recently, the above Lee and Pyun's theoretical results [61] have been confirmed by their experimental work using the Pd electrode with fractal surface [66].

Lithium transport under the cell-impedance-controlled constraint

From the theoretical [61] and experimental [66] studies conducted by Lee and Pyun introduced in the preceding section, one can obtain several qualitative results concerned with the mixed-controlled atom transport through the electrode with fractal surface. However, the application of those results is limited to the model system where the electrode potential curve follows the Nernst equation, so it is very difficult to actually utilise those results obtained from that work to the quantitative analysis of the experimental PCT and LSV measured from the specific systems.

In this respect, Go and Pyun's theoretical [64] and experimental [65] works may have attracted more attention to the researchers who devote themselves to investigating kinetics of mass transport in various systems. They examined how the surface roughness quantitatively affects lithium transport through the $Li_{1-\delta}CoO_2$ film electrode under cell-impedance-controlled constraint in a more realistic regime by using the numerical analysis of the GDE. They firstly derived the numerical solution to the GDE based upon the fractional calculus [76]. Before exploring their work, it should be recognised that when diffusion in the fractal media is governed by the GDE, the fractal-to-flat transition never occurs during atom transport even though the film thickness is long enough for the semi-infinite diffusion to occur.

Go and Pyun [64] theoretically computed the PCT and the LSV from the flat and fractal $Li_{1-\delta}CoO_2$ film electrodes by using the numerical solution to the GDE under the cell-impedance-controlled constraint at the electrode/electrolyte interface along with the impermeable constraint at the electrode/current collector interface. In their calculation, they took such simulation parameters as E, internal cell resistance R_{cell} and lithium diffusivity $\widetilde{D}_{Li}$ as the experimental data obtained directly from the fractal $Li_{1-\delta}CoO_2$ film electrode in their previous work [73].

The cell-impedance-controlled constraint at the electrode/electrolyte interface and the impermeable constraint at the electrode/current collector interface used in the calculation of the PCT and the LSV are given as:

$$\text{BC: } -zFA_{ea}\widetilde{D}_F(t)\left(\frac{\partial c(x,t)}{\partial x}\right)_{x=0} = \frac{\left(E_{app}-E(t)\right)}{R_{cell}} \quad \text{at } t>0 \quad (\text{cell}-\text{impedance}-\text{controlled constraint}) \tag{22}$$

$$\text{BC: } \left(\frac{\partial c(x,t)}{\partial x}\right)_{x=L} = 0 \text{ at } t>0 \quad (\text{impermeable constraint}) \tag{23}$$

In addition, $I(t)$ was calculated from the following equation which was obtained from the numerical analysis of Eq. (6):

$$I(t) = -zFA_{ea}\widetilde{D}_F(t)\left(\frac{\partial c(x,t)}{\partial x}\right)_{x=0} = zFA_{ea}\widetilde{D}_F(t)\frac{c(0,t)-c(\Delta x,t)}{\Delta x} \tag{24}$$

Figure 7 shows on a logarithmic scale the PCTs calculated from the flat and the fractal $Li_{1-\delta}CoO_2$ film electrodes by dropping E of 4.2 to 3.9 $V_{Li/Li+}$. The values of L and R_{cell} at 4.2 $V_{Li/Li+}$ are fixed as 2.0 μm and 10.0 Ω, respectively. All the PCTs exhibited the three-stage behaviour which accompanies the relatively long electrode under the cell-imped-

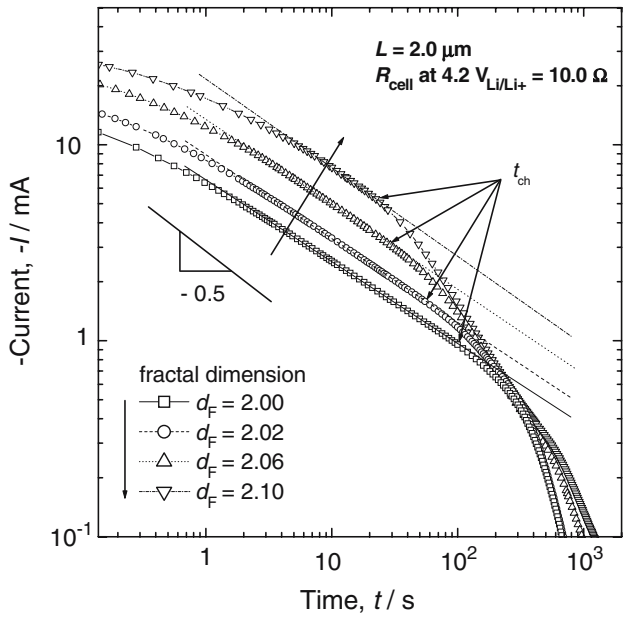

Fig. 7 Potentiostatic current transients calculated from the flat $Li_{1-\delta}CoO_2$ film electrode with d_F=2.0 and the fractal $Li_{1-\delta}CoO_2$ film electrodes with d_F=2.02, 2.06 and 2.10 by dropping the electrode potential of 4.2 to 3.9 $V_{Li/Li+}$ under the cell-impedance-controlled constraint at the electrode/electrolyte interface along with the impermeable constraint at the electrode/current collector interface. The values of the electrode thickness L and the internal cell resistance R_{cell} at 4.2 $V_{Li/Li+}$ are fixed as 2.0 μm and 10.0 Ω, respectively [64]

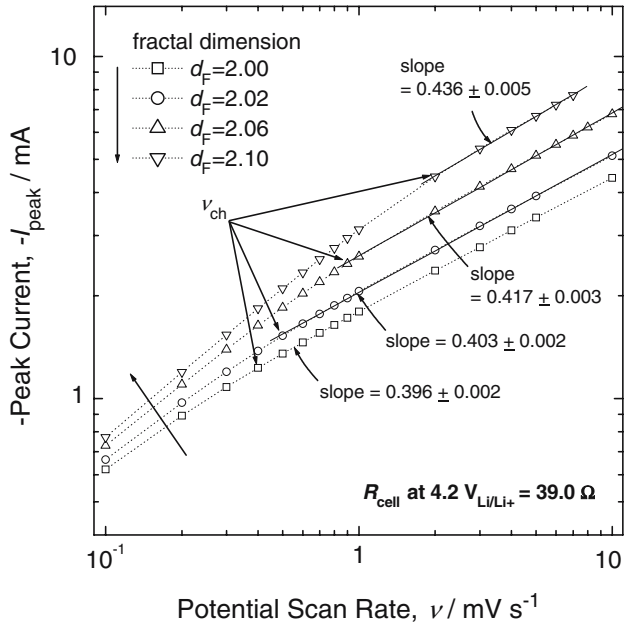

Fig. 8 Plots of the peak current I_{peak} vs the potential scan rate ν theoretically calculated from the flat $Li_{1-\delta}CoO_2$ film electrode with d_F=2.0 and the fractal $Li_{1-\delta}CoO_2$ film electrodes with d_F=2.02, 2.06 and 2.10 by scanning the applied potential from 4.3 to 3.5 $V_{Li/Li+}$ at various ν from 0.1 to 10 mV s^{-1} under the cell-impedance-controlled constraint at the electrode/electrolyte interface along with the impermeable constraint at the electrode/current collector interface. The values of the electrode thickness L and the internal cell resistance R_{cell} at 4.2 $V_{Li/Li+}$ are fixed as 5.0 μm and 39.0 Ω, respectively [64]

ance-controlled constraint: the logarithm of current decreased at first slowly with the logarithm of time, then it was proportional to the logarithm of time with a constant negative slope, and finally it decayed exponentially.

It should be emphasised that the linear relationship between the logarithms of current and time in the second stage, whose absolute value of the slope increases with increasing d_F, as well as the non-linear relationship in the first and third stages did not obey the generalised Cottrell equation presented in Eq. (12). In addition, as d_F increased, the values of I during the first and second stages and the time to transition of the second stage to the third stage increased and decreased, respectively.

The values of I_{peak}, which were obtained from the LSVs calculated from the fractal $Li_{1-\delta}CoO_2$ film electrodes with different d_F, are plotted against ν in Fig. 8 on a logarithmic scale. The values of L and R_{cell} at 4.2 $V_{Li/Li+}$ are fixed as 5.0 μm and 39.0 Ω, respectively. For all the electrodes, I_{peak} showed the power dependence on ν in the region of ν higher than the certain critical scan rate. However, it is clearly recognised that this power dependence negatively deviated from the generalised Randles–Sevcik relation expressed in Eq. (16). As d_F increased, I_{peak} and the critical scan rate as well as the power exponent just increased in value.

From the concentration profile transients of lithium across the $Li_{1-\delta}CoO_2$ film electrode, it was suggested that under the constraint of mixed control, the time to transition of the second stage to the third stage in the PCT of Fig. 7 and the critical scan rate of the plots of I_{peak} vs ν in Fig. 8 are caused by the transition of the semi-infinite diffusion to the finite diffusion and vice versa, respectively: namely, the time to transition of the second stage to the third stage in the PCT corresponds to the characteristic time t_{ch}, and the critical scan rate of the plots of I_{peak} vs ν corresponds just to the characteristic scan rate ν_{ch}.

Based upon the above suggestion, Go and Pyun [64] discussed the effect of the surface roughness on the cell-impedance-controlled lithium transport. In Figs. 7 and 8, as d_F increased, the values of t_{ch} and I until t_{ch} in the PCT decreased and increased, respectively, and the values of I_{peak} and ν_{ch} in the LSV just increased. This result means that the surface roughness enhances the cell-impedance-controlled lithium transport, and it is readily expected from the fact that the surface roughness markedly results in the increase in $\widetilde{D}_F(t)$ according to Eq. (7).

However, it should be noted that, in reality, the apparent increase in $\widetilde{D}_F(t)$ just implies the real increase in $A_F(t)$, i.e., electrochemically active area, since the GDE was derived by the mapping of diffusion towards fractal electrode with the time-dependent area $A_F(t)$ to one-dimensional Euclidean diffusion towards flat electrode with the time-independent constant area A_{ea} as shown in Eq. (8) [38]. Consequently, the enhancement of lithium transport due to the surface

roughness characterised by d_F is exclusively determined by the real increase in $A_F(t)$.

Furthermore, Go and Pyun [64] investigated the effect of R_{cell} on the cell-impedance-controlled lithium transport. Contrary to the effect of d_F on the lithium transport, as R_{cell} increased, the values of t_{ch} and I until t_{ch} in the PCT increased and decreased, respectively, and the values of I_{peak} and ν_{ch} in the LSV just decreased. From this fact, we can realise that the beneficial contribution of the surface roughness to the cell-impedance-controlled lithium transport counterbalances that detrimental contribution of the internal cell resistance. Recently, the above theoretical results of Go and Pyun [64] have been confirmed by their experimental work using the $Li_{1-\delta}CoO_2$ film electrodes with fractal surface [65].

Concluding remarks

In this review, anomalous diffusion towards and from fractal interface was explained for both diffusion-controlled and non-diffusion-controlled transfer processes. When diffusion is coupled with facile charge-transfer reaction, the electrochemical responses at fractal interface were treated with the help of the analytical solutions to the generalised diffusion equation (GDE). However, when diffusion is coupled with sluggish charge-transfer reaction, the description of the electrochemical responses at fractal interface was complicated.

In this respect, the theoretical [61, 64] and experimental [65, 66] studies of Pyun and his coworkers on atom transport through the intercalation electrode with fractal surface under the non-diffusion-controlled constraint may provide a guideline in analysing the electrochemical responses at fractal interface for non-diffusion-controlled transfer processes.

In conclusion, the numerical analysis of diffusion towards and from fractal interface can be widely used as a powerful tool to elucidate the transport phenomena of mass (ion for electrolyte and atom for intercalation electrode) across fractal interface whatever controls the overall transfer process.

Notation

A_{ea}	Time-independent electrochemically active area of flat interface (m^2)
$A_F(t)$	Time-dependent area of fractal interface (m^2)
b	Constant in Weierstrass function f_{WS}
$c(x,t)$	Local concentration of diffusing species (mol cm^{-3})
c^b	Bulk concentration of the diffusing species (mol cm^{-3})
$c_{Ox}(0,t)$	Surface concentration of Ox (mol cm^{-3})
$c_{Red}(0,t)$	Surface concentration of Red (mol cm^{-3})
$\widetilde{D}$	Chemical diffusivity of diffusing species ($cm^2\ s^{-1}$)
$\widetilde{D}_F(t)$	Time-dependent diffusivity ($cm^2\ s^{-1}$)
$\widetilde{D}_{Li}$	Lithium diffusivity ($cm^2\ s^{-1}$)
$\widetilde{D}*$	Fractional diffusivity $\left(cm^2 s^{d_F-3}\right)$
d_F	Fractal dimension
$d_{F,sa}$	Self-affine fractal dimension
$d_{F,ss}$	Self-similar fractal dimensions
d_W	Anomalous diffusion exponent
E	Electrode potential (V)
$E(t)$	Electrode potential as a function of the time t(V)
$E_{1/2}$	Half-wave potential (V)
E_{app}	Applied potential (V)
E_{ini}	Initial electrode potential (V)
E_{rev}	Reversible potential (V)
ΔE	Potential step (V)
F	Faraday constant (=96,487 C mol^{-1})
f	Dimensionless conversion factor
f_{WS}	Weierstrass function
I	Current (A)
$I(t)$	Current as a function of the time t (A)
I_0	Exchange current (A)
I_{app}	Applied current (A)
I_{peak}	Peak current (A)
$J(t)$	Macroscopic flow of an extensive quantity across fractal interface (mol $cm^{-2}\ s^{-1}$)
$J_E(x,t)$	Flow at planar interface given by Fick's first law (mol $cm^{-2}\ s^{-1}$)
$J_F(x,t)$	Flow at fractal interface (mol $cm^{-2}\ s^{-1}$)
K	Constant in the definition of the fractional diffusivity $\widetilde{D}^*$
K_0	Constant in the generalised transfer equation of Eq. (3)
k	Dimensionless constant in the definition of the time-dependent area of fractal interface $A_F(t)$
k^0	Rate constant of charge-transfer
N	Constant in Weierstrass function f_{WS}
R	Gas constant (=8.314 J $mol^{-1}\ K^{-1}$)
R_{cell}	Internal cell resistance (Ω)
T	Temperature (K)
t	Time (s)
t_{ch}	Characteristic time (s)
W_{tr}	Dimensionless jump probability of hydrogen
$\Delta X(t)$	Local driving force
x	Dimensionless hydrogen content in MH_x
x	Distance from fractal interface (m)

$Z_d(\omega)$	Diffusion impedance (Ω)
z	Valence of the diffusing species
Greek	
α	Transfer coefficient for hydrogen reduction
$(1-\alpha)$	Transfer coefficient for hydrogen oxidation
ε	Constant less than unity
$\Gamma(y)$	Gamma function of y
ν	Potential scan rate (V s^{-1})
ν_0	Slow threshold scan rate (V s^{-1})
ν_{ch}	Characteristic scan rate (V s^{-1})
θ	Phase angle
τ	Transition time (s)
τ_0	Temporal outer cut-off (s)
ω	Angular frequency
Mathematical operator	
*	Convolution operator
$\partial^\nu/\partial t^\nu$	Riemann–Liouville mathematical operator of a fractional derivative

Acknowledgements This research was supported by a grant from the Center for Advanced Materials Processing (CAMP) of the 21st Century Frontier R&D Program funded by the Ministry of Commerce, Industry and Energy (MOCIE), Republic of Korea. Furthermore, this work was partly supported by the Brain Korea 21 project.

References

1. Richardson LF (1926) Proc R Soc Lond A 110:709
2. Batchelor GK (1950) Q J Royal Meteorol Soc 76:133
3. Shlesinger MF, West BJ, Klafter J (1987) Phys Rev Lett 58:1100
4. Sokolov IM, Blumen A, Klafter J (1999) Europhys Lett 47:152
5. Scher H, Montroll EW (1973) Phys Rev B 7:4491
6. Scher H, Montroll EW (1975) Phys Rev B 12:2455
7. Pfister G, Scher H (1977) Phys Rev B 15:2062
8. Pfister G, Scher H (1978) Adv Phys 27:747
9. Zumofen G, Blumen A, Klafter J (1990) Phys Rev A 41:4558
10. Gu Q, Schiff EA, Grebner S, Schwartz R (1996) Phys Rev Lett 76:3196
11. Blom PWM, Vissenberg MCJM (1998) Phys Rev Lett 80:3819
12. Cardoso O, Tabeling P (1988) Europhys Lett 7:225
13. Amblard F, Maggs AC, Yurke B, Pargellis AN, Leibler S (1996) Phys Rev Lett 77:4470
14. Barkai E, Klafter J (1998) Phys Rev Lett 81:1134
15. Balescu R (1995) Phys Rev E 51:4807
16. Luedtke WD, Landman U (1999) Phys Rev Lett 82:3835
17. Bychuk OV, O'Shaugnessy B (1994) Phys Rev Lett 74:1795
18. Stapf S, Kimmich R, Seitter RO (1995) Phys Rev Lett 75:2855
19. Bodurka J, Seitter RO, Kimmich R, Gutsze A (1997) J Chem Phys 107:5621
20. Gefen Y, Aharony A, Alexander S (1983) Phys Rev Lett 50:77
21. O'Shaughnessy B, Procaccia I (1985) Phys Rev Lett 54:455
22. Harris AB, Aharony A (1987) Europhys Lett 4:1355
23. Giona M, Roman HE (1992) J Phys A Math Gen 25:2093
24. Giona M, Roman HE (1992) Physica A 185:87
25. Roman HE, Giona M (1992) J Phys A Math Gen 25:2107
26. Metzler R, Glöckle WG, Nonnenmacher TF (1994) Physica A 211:13
27. Vassilicos JC (1995) Phys Rev E 52:R5753
28. Metzler R, Nonnenmacher TF (1997) J Phys A Math Gen 30:1089
29. Le Mehaute A, Crepy G (1983) Solid State Ion 9–10:17
30. Le Mehaute A (1984) J Stat Phys 36:665
31. Nyikos L, Pajkossy T (1986) Electrochim Acta 31:1347
32. Nigmatullin RR (1986) Phys Status Solidi B 133:425
33. Pajkossy T, Nyikos L (1989) Electrochim Acta 34:171
34. Pajkossy T, Nyikos L (1989) Electrochim Acta 34:181
35. Nyikos L, Pajkossy T, Borosy AP, Martemyanov SA (1990) Electrochim Acta 35:1423
36. Borosy AP, Nyikos L, Pajkossy T (1991) Electrochim Acta 36:163
37. Pajkossy T, Borosy AP, Imre A, Martemyanov SA, Nagy G, Schiller R, Nyikos L (1994) J Electroanal Chem 366:69
38. Dassas Y, Duby P (1995) J Electrochem Soc 142:4175
39. Montroll EW, Weiss GH (1965) J Math Phys 6:167
40. Metzler R, Klafter J (2000) Phys Rep 339:1
41. West BJ, Grigolini P (2000) Fractional differences, derivatives and fractal time series. In: Hilfer R (ed) Applications of fractional calculus in physics. World Scientific, Singapore, pp 171–201
42. Lutz E (2001) Phys Rev Lett 86:2208
43. Ocon P, Herrasti P, Vázquez L, Salvarezza RC, Vara JM, Arvia AJ (1991) J Electroanal Chem 319:101
44. Pajkossy T (1991) J Electroanal Chem 300:1
45. Imre A, Pajkossy T, Nyikos L (1992) Acta Metall Mater 40:1819
46. Go JY, Pyun SI (2004) Electrochim Acta 49:2551
47. Strømme M, Niklasson GA, Granqvist CG (1995) Phys Rev B 52:14192
48. Strømme M, Niklasson GA, Granqvist CG (1995) Solid State Commun 96:151
49. Go JY, Pyun SI, Hahn YD (2003) J Electroanal Chem 549:49
50. Sapoval B (1987) Solid State Ion 23:253
51. Hill RM, Dissado LA (1988) Solid State Ion 26:295
52. Nyikos L, Pajkossy T (1990) Electrochim Acta 35:1567
53. Wyss W (1986) J Math Phys 27:2782
54. Schneider WR, Wyss W (1989) J Math Phys 30:134
55. Mainardi F (1996) Appl Math Lett 9:23
56. Záliš S, Fanelli N, Pospíšil L (1991) J Electroanal Chem 314:1
57. Záliš S, Pospíšil L, Fanelli N (1993) J Electroanal Chem 349:443
58. Pospíšil L, Záliš S, Fanelli N (1995) J Chem Educ 72:997
59. Zuo X, Xu C, Xin H (1997) Electrochim Acta 42:2555
60. Shin HC, Pyun SI, Go JY (2002) J Electroanal Chem 531:101
61. Lee JW, Pyun SI (2005) Electrochim Acta 50:1947
62. de Levie R, Vogt A (1990) J Electroanal Chem 281:23
63. Kant R, Rangarajan SK (1995) J Electroanal Chem 396:285
64. Go JY, Pyun SI (2005) Electrochim Acta 50:3479
65. Go JY, Pyun SI (2005) Electrochim Acta 50:5435
66. Lee JW, Pyun SI (2005) Electrochim Acta 51:694
67. Han JN, Seo M, Pyun SI (2001) J Electroanal Chem 499:152
68. Han JN, Lee JW, Seo M, Pyun SI (2001) J Electronal Chem 506:1
69. Pyun SI, Lee JW, Han JN (2002) J New Mater Electrochem Syst 5:243
70. Lee SJ, Pyun SI, Lee JW (2005) Electrochim Acta 50:1121
71. Lee JW, Pyun SI (2005) Electrochim Acta 50:1777
72. Shin HC, Pyun SI (1999) Electrochim Acta 45:489
73. Go JY, Pyun SI, Shin HC (2002) J Electroanal Chem 527:93
74. Shin HC, Pyun SI (2003) Mechanisms of lithium transport through transition metal oxides and carbonaceous materials. In: Vayenas CG, Conway BE, White RE (eds) Modern aspects of electrochemistry, no. 36. Plenum, New York, pp 255–301
75. Lee JW, Pyun SI (2004) Electrochim Acta 49:753
76. Podlubny I (1999) Fractional differential equations: an introduction to fractional derivatives, fractional differential equations, to methods of their solution and some of their applications. Academic, San Diego
77. Mandelbrot BB (1983) The fractal geometry of nature. Freeman, New York

78. Ho C, Raistrick ID, Huggins RA (1980) J Electrochem Soc 127:343
79. Jacobsen T, West K (1995) Electrochim Acta 40:255
80. Ding S, Petuskey WT (1998) Solid State Ion 109:101
81. Diard JP, Le Gorrec B, Montella C (1999) J Electroanal Chem 471:126
82. Bisquert J, Compte A (2001) J Electroanal Chem 499:112
83. Lee JW, Pyun SI (2005) Z Metallkd 96:2
84. Falconer K (1990) Fractal geometry: mathematical foundations and applications. Wiley, Chichester
85. Go JY, Pyun SI (2006) Fractal approach to rough surfaces and interfaces in electrochemistry. In: Vayenas CG, Conway BE, White Re (eds) Modern aspects of electrochemistry, Plenum, New York (in press)